Joule

CellPress

Article

Self-Selective Catalyst Synthesis for CO_2 Reduction

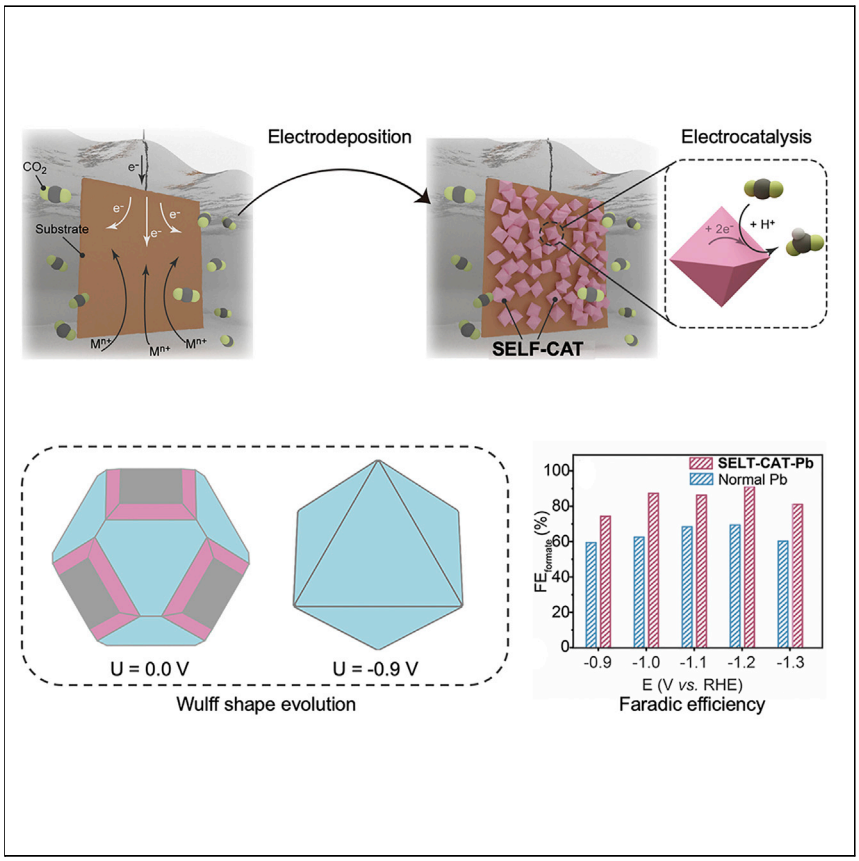

We developed a novel one-step simple method that introduces reactant during the synthesis process of metal nanoparticle. Taking the CO_2 electrochemical reduction reaction as an example, crystal morphology is modulated by intermediates generated from CO_2 reduction reaction, and the as-prepared material exhibits superior electrochemical catalytic performances toward CO_2RR. Computational results confirm that the reaction intermediates of CO_2RR could favorably stabilize the chosen facets, thus shaping the catalyst particles and facilitating the entire reduction reaction.

Hongxia Wang, Zheng Liang, Michael Tang, ..., Karen Chan, Tianwei Tan, Yi Cui

lianzhen@stanford.edu (Z.L.)
chank@stanford.edu (K.C.)
twtan@mail.buct.edu.cn (T.T.)
yicui@stanford.edu (Y.C.)

HIGHLIGHTS

A novel method of **SELF-CAT** was reported to rapidly identify a proper catalyst

Catalysts with specific morphology were synthesized because of CO_2 introduction

Intermediate of CO_2RR binds to the as preferred facet stronger

As-prepared **SELF-CAT** exhibits superior catalytic performance for CO_2RR

Wang et al., Joule 3, 1–10
August 21, 2019 Published by Elsevier Inc.
https://doi.org/10.1016/j.joule.2019.05.023

Please cite this article in press as: Wang et al., Self-Selective Catalyst Synthesis for CO_2 Reduction, Joule (2019), https://doi.org/10.1016/j.joule.2019.05.023

Joule

CellPress

Article

Self-Selective Catalyst Synthesis for CO_2 Reduction

Hongxia Wang,[1,2,6] Zheng Liang,[1,3,6,*] Michael Tang,[1,6] Guangxu Chen,[1] Yanbin Li,[1] Wei Chen,[1] Dingchang Lin,[1] Zewen Zhang,[1] Guangmin Zhou,[1] Jun Li,[1] Zhiyi Lu,[1] Karen Chan,[4,*] Tianwei Tan,[5,*] and Yi Cui[1,4,7,*]

SUMMARY

Catalysts play a significant role in many chemical processes to accelerate the reactions. However, the screening of a specific catalyst for one particular reaction usually requires elaborate procedures. Herein, we propose a novel concept of self-selective catalyst (SELF-CAT) to rapidly identify the proper catalyst for a certain chemical reaction by having the target reaction itself select its own catalyst. Electrochemical reduction of carbon dioxide (CO_2) is used as an example to demonstrate this method. Gaseous CO_2 is introduced and provides a surface-controlling agent to self-select and direct the crystal growth during the electrodeposition process, which is demonstrated by lead and copper. These resulting metal crystals thus possess a unique arrangement of crystal facets, which selectively binds the CO_2 reduction intermediates, exhibiting superior electrochemical catalytic performances. The preferential exposure of facets in the presence of CO_2 is furthermore suggested by density functional theory analysis.

INTRODUCTION

Catalyzed reactions form the basis of many industrial chemical processes. The selection of a proper catalyst for a particular chemical process remains challenging. We propose a novel strategy for rapid catalyst screening by having the chemical reaction select its own catalyst. Since the catalyst is selected by the target reaction itself, this screening strategy is self-selective. The resulting catalyst is defined as a self-selective catalyst (SELF-CAT). The self-selective method tends to stabilize the facets that bind the reactant intermediates the strongest since the adsorption of the reactants tends to lower the relative surface energies of these facets. In general, such an approach is applicable whenever stronger-binding or less coordinated facets are more active toward a particular reaction than the weaker-binding or more coordinated facets.

In order to demonstrate this concept of SELF-CAT, we now focus on an important chemical reaction: CO_2 reduction. Global climate change and energy demands underpin tremendous interest in the reductive transformation of carbon dioxide (CO_2) and water (H_2O) into value-added fuels and chemicals in a sustainable fashion.[1,2] Electroreduction of CO_2 into reduced carbon products powered by renewable electricity in aqueous electrolyte offers a cheap and environmentally benign route toward a carbon-neutral society.[3–8] Thus, of all the extensively investigated chemical processes, electrochemical reduction of CO_2 is studied as a starting point and example in this work.

Context & Scale

Catalysts are of vital importance for many chemical processes. Crystal facets have been known to exert a significant influence on the catalytic activity and selectivity. To tailor the surface morphology and select the optimal shape, traditional methods introduce additives and crystal modifiers during the materials synthesis process. In this work, we propose a novel strategy for rapid catalyst screening by having the chemical reaction select its own catalyst. The resulting modified metal crystals thus possess a unique arrangement of crystal facets, which selectively binds the reaction intermediates, exhibiting superior catalytic performances, which is demonstrated by lead and copper used in electrochemical CO_2 reduction reaction. Therefore, we anticipate this proposed screening approach searching for a proper catalyst will be applicable to a wide range of chemical processes in addition to CO_2 reduction, holding great potential for the future catalyst discovery and improvement.

Most catalysts for CO_2 reduction are transition and post-transition metals,[9–20] and the crystal facets have been known to exert a significant influence on the electrocatalytic activity and selectivity.[15,16,21–26] To tailor the surface morphology and select the optimal shape, traditional methods introduce electrolyte additives and crystal modifiers during the materials fabrication process.[21,27] Some successful examples using these additives include surfactants-controlled nanoparticles[28–31] with well-defined structures and better CO_2 catalytic performance, such as cubic copper (Cu) catalysts from the Anders Nilsson group[32] and a series of well-controlled shapes of nanoparticles from the Beatriz Cuenya group.[29] However, choosing a proper surfactant for specific material with a certain structure has many uncertain factors. These synthesis processes normally should be performed under harsh conditions. In addition, eliminating the residue surfactants after fabrication requires complex procedures and may result in notorious catalyst poisoning.[33] Instead of using extrinsic additives, our self-selective method can avoid the above problems by directly using the reactant itself (gaseous CO_2) and the resulting reduction intermediates to select the catalyst shape and achieve the optimum without further procedures.

In this present work, we apply our self-selective method on cost-effective transition metals for CO_2 reduction, such as lead (Pb) and Cu. These materials show weak-to-intermediate binding strengths for CO_2 reduction intermediates and hence are good candidates for this approach. As shown in Figure 1, to have CO_2 select its proper catalyst, the metal catalysts are synthesized by electrodeposition, and CO_2 is bubbled into the electrolyte till saturation to tune the particle facet exposure. We report herein the first observation of a morphology evolution during electrodeposition of the metal catalysts driven by the pre-adsorbed CO_2 molecules or its intermediates on the catalyst surface. This design was illustrated using Pb as an example. Specifically, in our experiment, metallic Pb grown with the aforementioned CO_2 modification in $PbNO_3$ electrolyte gradually evolves into octahedral morphology with a significant portion of (111) facets exposed, which is the first report on the synthesis of octahedral Pb nanoparticle. We therefore reasoned that during the electrodeposition of metal catalysts, CO_2 molecules are easily converted into some reduced intermediates on the catalyst surface under negative potentials as a surface-controlling agent. These adsorbed species such as polar carboxyl adsorbates, which are the intermediates of the CO_2 reduction reaction (CO_2RR), can have preferential binding effects with certain specific surfaces over others of the growing catalyst crystals and could function in the same way as that of the surfactant covered on metal nanocrystals. Therefore, they gradually tune the surface facet exposure in the entire catalyst synthesis process, giving rise to highly active and stable catalysts for CO_2 reduction. Under CO_2 reduction conditions, these self-selective Pb catalysts (**SELF-CAT-Pb**) with the CO_2's chosen facets, (111), exhibit a great increase in activity compared with the normal Pb without CO_2 tuning, from many perspectives, and outperforming state-of-the-art CO_2 electrocatalysts based on the same metal.[34] Moreover, density functional theory (DFT) calculations were conducted, and the simulations confirm that the Pb(111) facet selected by CO_2 itself stabilizes carboxyl species (CO_2RR intermediates) more effectively and can be more favorable for liquid product formation.

RESULTS AND DISCUSSION

The material characterizations of **SELF-CAT-Pb** and the corresponding catalytic performance of CO_2 reduction are shown in Figure 2. The tested samples are electrodeposited onto three-dimensional carbon fiber papers under a saturated argon (Ar) condition for normal Pb and a saturated CO_2 condition for **SELF-CAT-Pb**.

[1]Department of Materials Science and Engineering, Stanford University, Stanford, CA 94305, USA

[2]Beijing Advanced Innovation Center for Soft Matter Science and Engineering, Beijing University of ChemicalTechnology, Beijing 100029, China

[3]School of Chemistry and Chemical Engineering, Shanghai Jiao Tong University, Shanghai 200240, China

[4]Stanford Institute for Materials and Energy Sciences, SLAC National Accelerator Laboratory, 2575 Sand Hill Road, Menlo Park, CA 94025, USA

[5]National Energy R&D Center for Biorefinery, Beijing University of Chemical Technology, Beijing 100029, China

[6]These authors contributed equally

[7]Lead Contact

*Correspondence: lianzhen@stanford.edu (Z.L.), chank@stanford.edu (K.C.), twtan@mail.buct.edu.cn (T.T.), yicui@stanford.edu (Y.C.)

https://doi.org/10.1016/j.joule.2019.05.023

Please cite this article in press as: Wang et al., Self-Selective Catalyst Synthesis for CO_2 Reduction, Joule (2019), https://doi.org/10.1016/j.joule.2019.05.023

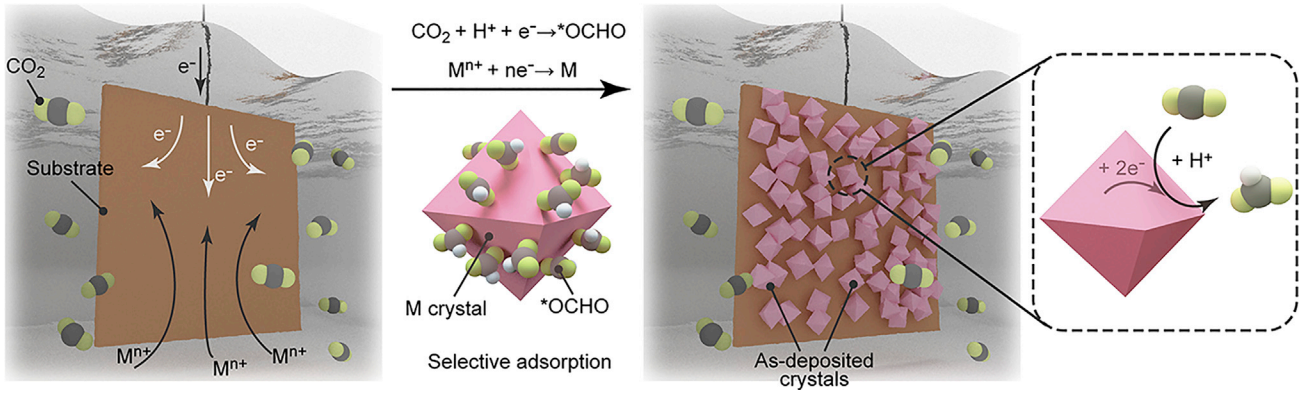

Figure 1. Schematics of the SELF-CAT with Particular Surfaces Favoring CO_2RR

This design is illustrated using metallic lead as an example. Specifically, lead crystals were electrodeposited onto a conductive substrate from a Pb^{2+} cation containing electrolyte continuously purged with CO_2. Meanwhile, the adsorbed CO_2 molecules under this electrodeposition potential will be slightly reduced to polar carboxyl species. These resulting carboxyl adsorbates selectively interact with specific facets of the growing metal crystal and function as surface-controlling agents. The as-formed CO_2-tuned lead crystals with a unique shape exhibit excellent activity when used as catalysts for CO_2 reduction.

Morphology for both samples was investigated by scanning electron microscopy (SEM) (Figures 2A–2D), indicating that the particle shape is highly dependent on the electrodeposition atmosphere. Pb particles formed in the absence of electrolyte additives under Ar atmosphere (normal Pb) possess irregular shape with a random combination of several facets (Figures 2A and 2B). In contrast, Pb particles prepared under saturated CO_2 atmosphere (**SELF- CAT-Pb**) feature a well-defined octahedral shape with sidewalls corresponding to the Pb (111) facet (Figures 2C and 2D), which can be confirmed from a comparison between typical **SELF-CAT-Pb** particles and a standard octahedron (Figure S1). Specifically, several typical **SELF-CAT-Pb** particles at random orientation were chosen, and a standard, well-defined octahedron with eight (111) surfaces was used to match the above **SELF-CAT-Pb** particles. The surfaces of these **SELF-CAT-Pb** particles can therefore be proved to be Pb(111) facets from this perfect match (Figure S1). These octahedral particles can be observed clearly under high magnification as displayed in the inset image of Figure 2D. Furthermore, the SEM images under low magnification (Figure S2) clearly show that Pb particles are well distributed on the carbon fiber paper. To further confirm this morphology evolution and analyze the exposed facets of **SELF-CAT**, Pb crystals were deposited and studied by X-ray diffraction (XRD). For normal Pb and **SELF-CAT- Pb**, it is clear that both patterns match well with the standard Pb peaks (Joint Committee on Powder Diffraction Standards [JCPDS] No. 65-2873). Nevertheless, the relative peak intensities of the three most intense reflections (111), (200), and (220) differ from each other (Figure 2E). Furthermore, the texture coefficient (TC) of the three major reflection planes (111), (200), and (220) was calculated to quantitatively predict the degree of preferred crystal orientation according to Harris formula.[35] The TC value of Pb(111) increases from 0.18 to more than 1 (Figure S3) from normal Pb to **SELF-CAT-Pb**. These results reveal that during the electrodeposition, CO_2 molecules could function as a surface-controlling agent and gradually stabilize an octahedral morphology for Pb, selectively exposing primarily (111) facets. Moreover, instead of fabricating the Pb particles from a Pb^{2+}-containing solution, we also tested electrochemical reduction of solid Pb precursor such as lead oxide (PbO) in several different liquid electrolytes, confirming the feasibility of this self-selection method under various environments. The morphology of Pb particles formed under the Ar versus CO_2 condition using an electrolyte other than $PbNO_3$ was presented as Figure S4. All the Pb particles exhibit similar tendency in

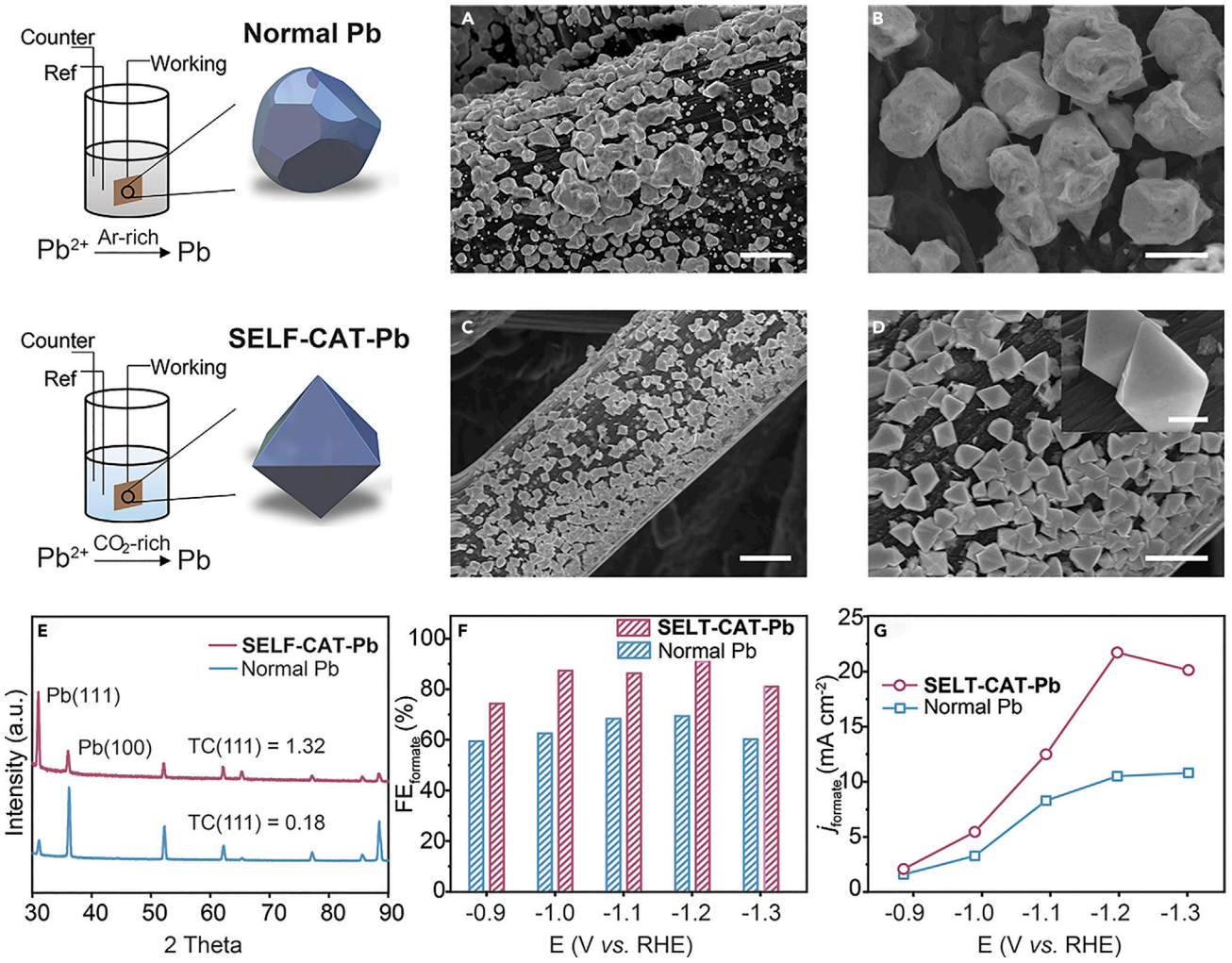

Figure 2. Morphology and Corresponding Electrocatalytic Properties of Lead-Based Catalysts for CO_2 Reduction

(A and B) Low-magnification (A) and high-magnification (B) SEM images of normal Pb particles.

(C and D) Low-magnification (C) and high-magnification (D) SEM images of **SELF-CAT-Pb** particles.

(E) XRD pattern of normal Pb particles and **SELF-CAT-Pb** particles.

(F) Comparison of formate FE for lead-based catalysts under various potentials.

(G) Comparison of calculated formate partial current density based on geometric surface area of lead-based catalysts under various potentials.

Scale bars in Figures 2A and 2C, 2 μm. Scale bars in Figures 2B and 2D, 1 μm. Scale bars in the inset, 200 nm.

morphology evolution under the influence of CO_2, regardless of the electrolyte environment, as well as the precursor, which proves that the function of CO_2 applies effectively in a universal way. In addition, the possibility of carbonate species, pH changing, combined gases, electrodeposition voltage, and electrodeposition time thus suggests that the morphology evolution cannot be attributed to these factors (Table S1; Figures S5–S9).

According to the above SEM and XRD studies, Pb(111) facets are the preferred crystal facets as a result of the selection by CO_2. Electrocatalytic characterizations were then carried out to examine the catalytic activity of this chosen crystal plane. All the testing potentials are referenced to the standard calomel electrode (SCE) (conversion into reversible hydrogen electrode [RHE] is shown in the Supplemental Information). Figure S10 shows cyclic voltammetry (CV) curves for Pb-based

catalysts. The **SELF-CAT-Pb** catalyst exhibits larger total current densities relative to its counterparts, and this difference increases in the more negative voltage range (< −0.9 V versus RHE), suggesting the improved CO_2 reduction activity.[23] Controlled potential electrolysis was performed in CO_2-saturated potassium bicarbonate electrolyte under applied potentials from −0.9 to −1.3 V versus RHE in order to further examine the CO_2 reduction behavior. Liquid products were quantified by nuclear magnetic resonance (NMR) spectroscopy, and the gas products were analyzed by gas chromatography (GC). The major CO_2RR products of Pb catalysts are C_1 products, including formate and hydrogen (competitive proton reduced gaseous product). The faradic efficiency (FE) of reduction products is shown in Figure 2F (formate) and Figure S11 (hydrogen). The **SELF-CAT- Pb** shows higher formate FE compared with normal Pb of the entire examined potential window. At −1.2 V versus RHE, the **SELF-CAT-Pb** displays optimal performance for formate (FE = 90.5%) and significantly suppressed hydrogen evolution (FE of hydrogen evolution < 10%) (Figure S11). Since product selectivity can be rationalized through the binding energy differences of intermediates,[36] the poor hydrogen evolution behavior can be attributed to the weak interaction between protons and Pb(111) (Table S2), suggesting a more favored CO_2RR on this chosen facet. Nevertheless, at the same applied reduction potential, normal Pb catalyst exhibits a formate FE of 69%, and a more than 30% charge was devoted to hydrogen production (Figure 2F). This enhancement can be quantified as shown in the NMR analysis (Figure S12).

Figure 2G presents the geometric partial current density of formate. This partial current density was calculated from the total current density (Figure S13) and formate selectivity (Figure 2F). For **SELF-CAT-Pb**, the obtained formate current density ($j_{formate}$) at −1.2 V versus RHE reached to around 22 mA/cm^2, whereas $j_{formate}$ of normal Pb was only 10.4 mA/cm^2 at the same applied potential. The increased formate partial current density indicates an enhanced CO_2 reduction ability of **SELF-CAT-Pb** with the CO_2's chosen facets.[37] The electrochemical active surface area (ECSA) for normal Pb and **SELF-CAT-Pb** was also compared by measuring the capacitive current associated with double-layer charging from the scan-rate dependence of CVs (Figure S14). As shown in Figure S14, the linear slopes are almost the same for both normal Pb and **SELF- CAT-Pb**, indicating a similar ECSA.[38] Therefore, the differences in geometric current densities can be attributed to differences in intrinsic activity (Figure S15).

The long-term catalytic behavior was also examined. Hydrogen evolution was continuously monitored by GC over the entire process at −1.2 V versus RHE as an indicator of formate selectivity. Although the formate selectivity shows a slight decrease with increasing catalysis time, the overall formate FE over the course of 6 h stays around 86% (Figure S16). In addition, the total reduction current density remains relatively stable at ~22 mA/cm^2 (Figure S16), indicating the excellent long-term stability of this **SELF-CAT-Pb** with the CO_2's chosen (111) facets. Another critical measure for the long-term catalytic stability is the post-catalysis SEM characterization. As shown in Figure S17, the octahedral shape of the **SELF-CAT-Pb** is well maintained even after 6 h of catalysis, which may explain the stable reduction current and formate selectivity. To conclude, the improvement of CO_2 reduction catalytic activity and, specifically, the formate selectivity, is consistent with our hypothesis suggesting facile CO_2 reduction energetics on the CO_2-selected Pb(111) facets. This hypothesis will then be confirmed by computation studies in the following part.

To further confirm our hypothesis on the morphology evolution and performance enhancement resulted from the self-selection, as well as examine the energetics of

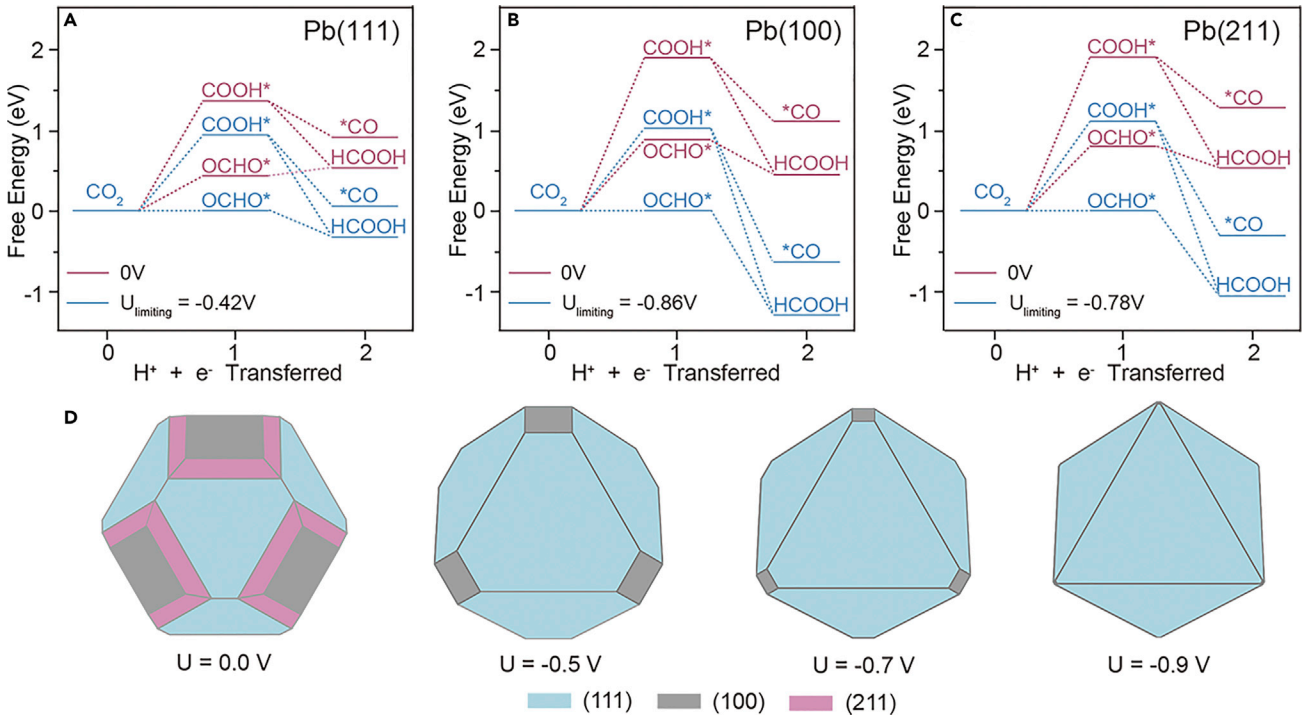

Figure 3. Free-Energy Diagrams for the Energetics of CO_2RR

(A) Free-energy diagram of CO_2RR on Pb(111) facet.

(B) Free-energy diagram of CO_2RR on Pb(100) facet.

(C) Free-energy diagram of CO_2RR on Pb(211) facets. The red lines represent energy diagram at 0 V versus RHE, and the blue lines represent energy diagram at the corresponding limiting potentials, which are the minimum potentials required to initiate the CO_2RR on each facet. Each step along the horizontal axis refers to the transfer of a proton from electrolyte and an electron from the electrode to the adsorbates.

(D) Wulff shape evolution as a function of potential arising from the surface energy changes shown in Figure S18. The facets are color coded as such: light blue (111), gray (100), and pink (211).

the chosen facets, computational studies using DFT and the computational hydrogen electrode were carried out. Binding energies were calculated with H_2O as the oxygen reference species, H_2 as the hydrogen reference species, and CO_2 as the carbon reference species. Revised Perdew-Burke-Ernzerhof (RPBE) functional was chosen as the exchange-correlation functional, as it has been shown to yield accurate chemisorption energetics over a large number of well-known, experimentally measured chemisorption cases.[39] Typically, in the face-centered-cubic (FCC) Pb system, (111) and (100) are the dominating crystal planes according to the Crystalium.[40] In addition, we also consider (211) as a model facet for stepped sites. The resulting free-energy diagrams (Figures 3A–3C) show the CO_2 reduction pathways on the above three facets toward CO and HCOOH, the two possible 2-electron products. In general, COOH is the intermediate toward CO, while HCOOH can be formed from either COOH or OCHO. The OCHO is thermodynamically more favorable than COOH on all three facets, suggesting the OCHO species to be the critical reaction intermediate for CO_2RR and rationalizes the high selectivity toward HCOOH versus CO. The trend showing OCHO as the preferred pathway is in agreement with past literature[41] despite binding energy strengths differing by around −0.5 eV because of exchange-correlation functional differences. The binding energy of OCHO was found to be strongest with Pb(111) where the oxygen atoms bind atop 2 closely packed Pb surface atoms. The binding energy of OCHO was found to be weaker on (100) and (211) presumably because the size of Pb atoms leaves larger

bonding distances for OCHO molecules to adsorb well over these facets. The resultant limiting potentials on the (111), (100), and (211) facets are −0.42, −0.86, and −0.78 V, respectively, versus RHE, suggesting the Pb(111) facet to be the most active for HCOOH production.

We further considered the variation in surface energy of the various facets in the CO_2-rich environment during the synthesis. Our method allowed us to estimate the coverage of intermediates as a function of potential. Since surface reconstruction is driven by chemisorption,[42] we then modified surface energetics to reflect the coverage at a given potential. Figure S18 shows the variation of surface energies with *OCHO at intermediate coverages of 12.5% and 25% as a function of potential. The corresponding evolution in Wulff particle shapes is shown in Figure 3D. While the *OCHO coverage is ultimately determined by kinetics, the current analysis suggests that the presence of CO_2 and a reducing applied potential would favor the formation of Pb(111) facets. Figure S19 shows the evolution in the Pb(111) area fraction with applied potential. The theoretical analysis suggests that under a CO_2 atmosphere and applied potential of −0.5V versus RHE, the area fraction of Pb(111) is nearly doubled.

Besides Pb, the concept of **SELF-CAT** was also applied to Cu to show its feasibility as a universal strategy. Figure 4A shows the normal Cu particles with a random shape, while Figure 4B shows the **SELF-CAT- Cu** particles. It is clearly shown that there is a large portion of Cu steps in the **SELF-CAT-Cu** compared with its counterpart. This existence of Cu steps as a result of CO_2's selection can also be confirmed from the XRD pattern (Figure 4C). Compared with standard Cu pattern (JCPDS No. 4-836) for normal Cu, intensities of diffraction peaks indexed as Cu(111), Cu(220), and Cu(311) are largely increased for **SELF-CAT-Cu**, indicating the Cu steps as the CO_2's chosen morphology.[43] According to the literature,[44] carbon monoxide, as a CO_2RR intermediate, is proven to have strong interactions with Cu-stepped surfaces. We thus reasoned that polar CO molecules can function as a surface-controlling agent to modify the Cu particle shape, which is analogous to the effect of OCHO on Pb. Under this assumption, the shape evolution can be demonstrated from the Wulff shape as shown in Figures 4D and 4E. The Wulff shapes of the Cu nanoparticles are based on a previous manuscript that followed similar computational steps in creating Wulff shapes.[45] Figure 4D presents the clean Cu particle with various facets. Figure 4E presents the shape after being exposed under a minimal CO partial pressure of around 4.4×10^{-9} bars. It is clearly shown that the portion of Cu steps increases noticeably in the presence of CO.[43,44] As for the electrocatalytic performance, according to the CV curves (Figure S20), this modified **SELF-CAT-Cu** exhibits a larger current density compared with normal Cu, indicating an enhanced catalytic activity. Moreover, this **SELF-CAT-Cu** also shows a superior liquid product selectivity with formate FE increasing from 27% to 54.5% at −0.7 V versus RHE and a higher selectivity with C_{2+} products from 20.9% to 42.2% at −1.0 V versus RHE in comparison with its counterpart, the normal Cu (Figure 4F). The **SELF-CAT-Cu** would suppress the hydrogen obviously, which agrees with previous studies revealing that CO_2RR is more favored on Cu steps than other surfaces.[44] The ECSA measurements then reveal a similar electro-active surface area for both normal Cu and **SELF-CAT-Cu**, proving the intrinsic nature of this activity improvement (Figures S21 and S22). Besides, long-term catalysis (−1.0 V versus RHE) was also performed (Figure S23), and the morphology after a 6 h CO_2RR (Figure S24) was examined for both normal and **SELF-CAT-Cu** catalysts. The electrocatalytic and structural stability of this **SELF-CAT-Cu** can therefore be confirmed from the stable current curve as well as the intact morphology after reduction.

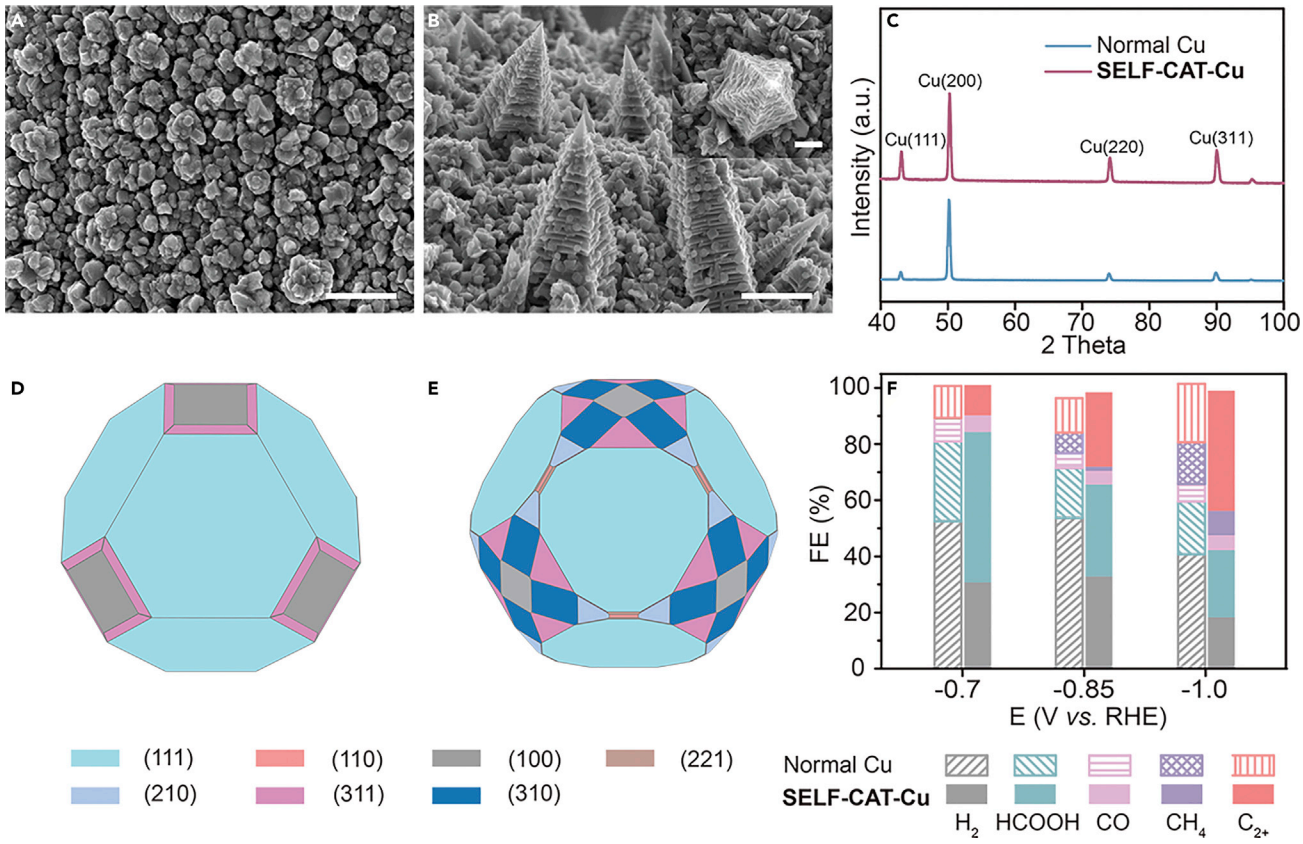

Figure 4. Material Characterizations and Electrocatalytic Properties of Copper-Based Catalysts for CO_2 Reduction

(A) SEM images of normal Cu particles.

(B) SEM images of **SELF-CAT-Cu** particles.

(C) XRD patterns of normal Cu and **SELF-CAT-Cu**.

(D and E) Wulff shape of copper crystals showing the shape evolution under effect of CO, where p(CO) is around 4.4×10^{-9} bar. (D) Clean copper crystal.

(E) Simulated copper crystal after exposed with CO.

(F) Comparison of reduction product FE for copper-based catalysts under various potentials. Scale bars in Figures 4A and 4B, 500 nm. Scale bars in the inset, 100 nm.

Therefore, in addition to Pb, the resulting **SELF-CAT-Cu** also exhibits a unique shape and superior catalytic activity using this method. The self-selection strategy applies well to Cu.

In summary, for a CO_2 reduction catalyst, its catalytic performance depends highly on the catalyst morphology. Instead of synthesizing and examining multiple candidates, we herein report an innovative and easily scalable approach (self-selection) enabling CO_2 itself to select its preferred catalyst. This self-selective method tends to stabilize the catalyst's facets that bind the reactant intermediates the strongest since the adsorption of the reactants tends to lower the relative surface energies of these facets. The as-formed catalyst exhibits a significant portion of the chosen crystal planes, selected by the reaction intermediates, and converts CO_2 into useful liquid products during reduction effectively. We have demonstrated a novel approach to maximize the exposure of a certain facet for the desired CO_2 reduction path tested by two catalytic materials (Pb and Cu). In addition, computational results confirm that the reaction intermediates of CO_2RR could favorably stabilize the chosen facets, thus shaping the catalyst particles and facilitating the entire reduction reaction. In general, such an approach is applicable whenever stronger-binding or

less coordinated facets are more active toward a particular reaction than the weaker-binding or more coordinated facets. We therefore anticipate this proposed screening approach to searching for a proper catalyst will be applicable to a wide range of chemical processes as a general way to tune and improve a metal catalyst with desired properties, holding great potential for future catalyst discovery and improvement.

EXPERIMENTAL PROCEDURES

Details of all experimental procedures can be found in the Supplemental Information.

SUPPLEMENTAL INFORMATION

Supplemental Information can be found online at https://doi.org/10.1016/j.joule.2019.05.023.

ACKNOWLEDGMENTS

This work was initiated by the support of the Department of Energy, Office of Basic Energy Sciences, Materials Sciences and Engineering Division under contract DEAC02-76-SF00515. We acknowledge the use and support of the Stanford Nano Shared Facilities (SNSF) for sample characterization. Theoretical calculations were based upon work performed by the Joint Center for Artificial Photosynthesis, a DOE Energy Innovation Hub, supported through the Office of Science of the U.S. Department of Energy under award number DE-SC0004993. H.W. acknowledges the funding support from the National Postdoctoral Program for Innovative Talents (grant BX201600011). T.T. acknowledge the support from the National Basic Research Program of China (973 program: 2013CB733600) and the National Nature Science Foundation of China (grant no. 21436002).

AUTHOR CONTRIBUTIONS

H.W., Z. Liang, M.T., K.C., T.T., and Y.C. conceived the research. Z. Liang, H.W., G.C., Y.L., W.C., Z.Z., D.L., G.Z., J.L., and Z. Lu. performed the experiments. M.T. and K.C. performed the theoretical calculation. H.W., Z. Liang, M.T., K.C., and Y.C. analyzed the data. H.W., Z. Liang, M.T., K.C., and Y.C. prepared the manuscript with input from all the other coauthors.

DECLARATION OF INTERESTS

The authors declare no competing interests.

Received: March 4, 2019
Revised: April 27, 2019
Accepted: May 23, 2019
Published: June 18, 2019

REFERENCES

1. Lewis, N.S., and Nocera, D.G. (2006). Powering the planet: chemical challenges in solar energy utilization. Proc. Natl. Acad. Sci. USA *103*, 15729–15735.

2. Gray, H.B. (2009). Powering the planet with solar fuel. Nat. Chem. *1*, 7.

3. Costentin, C., Robert, M., and Savéant, J.M. (2013). Catalysis of the electrochemical reduction of carbon dioxide. Chem. Soc. Rev. *42*, 2423–2436.

4. Liu, C., Colón, B.C., Ziesack, M., Silver, P.A., and Nocera, D.G. (2016). Water splitting–biosynthetic system with CO_2 reduction efficiencies exceeding photosynthesis. Science *352*, 1210–1213.

5. Concepcion, J.J., House, R.L., Papanikolas, J.M., and Meyer, T.J. (2012). Chemical approaches to artificial photosynthesis. Proc. Natl. Acad. Sci. USA *109*, 15560–15564.

6. Sakimoto, K.K., Wong, A.B., and Yang, P. (2016). Self-photosensitization of nonphotosynthetic bacteria for solar-to-chemical production. Science *351*, 74–77.

7. Wang, H., Chen, Y., Hou, X., Ma, C., and Tan, T. (2016). Nitrogen-doped graphenes as efficient electrocatalysts for the selective reduction of

carbon dioxide to formate in aqueous solution. Green Chem. *18*, 3250–3256.

8. Li, J., Chen, G., Zhu, Y., Liang, Z., Pei, A., Wu, C.-L., Wang, H., Lee, H.R., Liu, K., Chu, S., et al. (2018). Efficient electrocatalytic CO_2 reduction on a three-phase interface. Nat. Catal. *1*, 592–600.

9. Li, C.W., Ciston, J., and Kanan, M.W. (2014). Electroreduction of carbon monoxide to liquid fuel on oxide-derived nanocrystalline copper. Nature *508*, 504–507.

10. Hori, Y. (2008). Electrochemical CO_2 reduction on metal electrodes in modern aspects of electrochemistry, C.G. Vayenas, R.E. White, and M.E. Gamboa-Aldeco, eds. (Springer New York), pp. 89–189.

11. Wuttig, A., Yoon, Y., Ryu, J., and Surendranath, Y. (2017). Bicarbonate is not a general acid in Au-catalyzed CO_2 electroreduction. J. Am. Chem. Soc. *139*, 17109–17113.

12. Liu, M., Pang, Y., Zhang, B., De Luna, P., Voznyy, O., Xu, J., Zheng, X., Dinh, C.T., Fan, F., Cao, C., et al. (2016). Enhanced electrocatalytic CO_2 reduction via field-induced reagent concentration. Nature *537*, 382–386.

13. Lu, Q., Rosen, J., Zhou, Y., Hutchings, G.S., Kimmel, Y.C., Chen, J.G., and Jiao, F. (2014). A selective and efficient electrocatalyst for carbon dioxide reduction. Nat. Commun. *5*, 3242.

14. Kim, C., Jeon, H.S., Eom, T., Jee, M.S., Kim, H., Friend, C.M., Min, B.K., and Hwang, Y.J. (2015). Achieving selective and efficient electrocatalytic activity for CO_2 reduction using immobilized silver nanoparticles. J. Am. Chem. Soc. *137*, 13844–13850.

15. Reske, R., Mistry, H., Behafarid, F., Roldan Cuenya, B., and Strasser, P. (2014). Particle size effects in the catalytic electroreduction of CO_2 on Cu nanoparticles. J. Am. Chem. Soc. *136*, 6978–6986.

16. Gao, D., Zhou, H., Wang, J., Miao, S., Yang, F., Wang, G., Wang, J., and Bao, X. (2015). Size-dependent electrocatalytic reduction of CO_2 over Pd nanoparticles. J. Am. Chem. Soc. *137*, 4288–4291.

17. Zhang, S., Kang, P., and Meyer, T.J. (2014). Nanostructured tin catalysts for selective electrochemical reduction of carbon dioxide to formate. J. Am. Chem. Soc. *136*, 1734–1737.

18. Gao, S., Gu, B., Jiao, X., Sun, Y., Zu, X., Yang, F., Zhu, W., Wang, C., Feng, Z., Ye, B., et al. (2017). Highly efficient and exceptionally durable CO_2 photoreduction to methanol over freestanding defective single-unit-cell bismuth vanadate layers. J. Am. Chem. Soc. *139*, 3438–3445.

19. DiMeglio, J.L., and Rosenthal, J. (2013). Selective conversion of CO_2 to CO with high efficiency using an inexpensive bismuth-based electrocatalyst. J. Am. Chem. Soc. *135*, 8798–8801.

20. Lin, S., Diercks, C.S., Zhang, Y.B., Kornienko, N., Nichols, E.M., Zhao, Y., Paris, A.R., Kim, D., Yang, P., Yaghi, O.M., et al. (2015). Covalent organic frameworks comprising cobalt porphyrins for catalytic CO_2 reduction in water. Science *349*, 1208–1213.

21. Zhao, J., Sun, L., Canepa, S., Sun, H., Yesibolati, M.N., Sherburne, M., Xu, R., Sritharan, T., Loo, J.S.C., Ager, J.W., III, et al. (2017). Phosphate tuned copper electrodeposition and promoted formic acid selectivity for carbon dioxide reduction. J. Mater. Chem. A *5*, 11905–11916.

22. Luo, W., Nie, X., Janik, M.J., and Asthagiri, A. (2016). Facet dependence of CO_2 reduction paths on Cu electrodes. ACS Catal. *6*, 219–229.

23. Cai, F., Gao, D., Zhou, H., Wang, G., He, T., Gong, H., Miao, S., Yang, F., Wang, J., and Bao, X. (2017). Electrochemical promotion of catalysis over Pd nanoparticles for CO_2 reduction. Chem. Sci. *8*, 2569–2573.

24. Huang, X., Tang, S., Mu, X., Dai, Y., Chen, G., Zhou, Z., Ruan, F., Yang, Z., and Zheng, N. (2011). Freestanding palladium nanosheets with plasmonic and catalytic properties. Nat. Nanotechnol. *6*, 28–32.

25. Pan, Y., Lin, R., Chen, Y., Liu, S., Zhu, W., Cao, X., Chen, W., Wu, K., Cheong, W.-C., Wang, Y., et al. (2018). Design of single-atom Co–N_5 catalytic site: A robust electrocatalyst for CO_2 reduction with nearly 100% CO selectivity and remarkable stability. J. Am. Chem. Soc. *140*, 4218–4221.

26. Wang, X., Choi, S.-I., Roling, L.T., Luo, M., Ma, C., Zhang, L., Chi, M., Liu, J., Xie, Z., Herron, J.A., et al. (2015). Palladium–platinum core-shell icosahedra with substantially enhanced activity and durability towards oxygen reduction. Nat. Commun. *6*, 7594.

27. Siegfried, M.J., and Choi, K.-S. (2008). Elucidation of an overpotential-limited branching phenomenon observed during the electrocrystallization of cuprous oxide. Angew. Chem. Int. Ed. *47*, 368–372.

28. Habas, S.E., Lee, H., Radmilovic, V., Somorjai, G.A., and Yang, P. (2007). Shaping binary metal nanocrystals through epitaxial seeded growth. Nat. Mater. *6*, 692–697.

29. Mostafa, S., Behafarid, F., Croy, J.R., Ono, L.K., Li, L., Yang, J.C., Frenkel, A.I., and Cuenya, B.R. (2010). Shape-dependent catalytic properties of Pt nanoparticles. J. Am. Chem. Soc. *132*, 15714–15719.

30. Peng, Z., and Yang, H. (2009). Designer platinum nanoparticles: control of shape, composition in alloy, nanostructure and electrocatalytic property. Nano Today *4*, 143–164.

31. Shevchenko, E.V., Talapin, D.V., Kotov, N.A., O'Brien, S., and Murray, C.B. (2006). Structural diversity in binary nanoparticle superlattices. Nature *439*, 55–59.

32. Roberts, F.S., Kuhl, K.P., and Nilsson, A. (2015). High selectivity for ethylene from carbon dioxide reduction over copper nanocube electrocatalysts. Angew. Chem. Int. Ed. *54*, 5179–5182.

33. Susman, M.D., Feldman, Y., Vaskevich, A., and Rubinstein, I. (2014). Chemical deposition of Cu_2O nanocrystals with precise morphology control. ACS Nano *8*, 162–174.

34. Zhu, Q., Ma, J., Kang, X., Sun, X., Liu, H., Hu, J., Liu, Z., and Han, B. (2016). Efficient reduction of CO_2 into formic acid on a lead or tin electrode using an ionic liquid catholyte mixture. Angew. Chem. Int. Ed. *55*, 9012–9016.

35. Liu, J., Duan, J.L., Toimil-Molares, M.E., Karim, S., Cornelius, T.W., Dobrev, D., Yao, H.J., Sun, Y.M., Hou, M.D., Mo, D., et al. (2006). Electrochemical fabrication of single-crystalline and polycrystalline Au nanowires: the influence of deposition parameters. Nanotechnology *17*, 1922–1926.

36. Shi, C., Hansen, H.A., Lausche, A.C., and Nørskov, J.K. (2014). Trends in electrochemical CO_2 reduction activity for open and close-packed metal surfaces. Phys. Chem. Chem. Phys. *16*, 4720.

37. Choi, S.Y., Jeong, S.K., Kim, H.J., Baek, I.-H., and Park, K.T. (2016). Electrochemical reduction of carbon dioxide to formate on tin–lead alloys. ACS Sustainable Chem. Eng. *4*, 1311–1318.

38. Song, F., and Hu, X. (2014). Ultrathin cobalt–manganese layered double hydroxide is an efficient oxygen evolution catalyst. J. Am. Chem. Soc. *136*, 16481–16484.

39. Hammer, B., Hansen, L.B., and Nørskov, J.K. (1999). Improved adsorption energetics within density-functional theory using revised Perdew-Burke-Ernzerhof functionals. Phys. Rev. B *59*, 7413–7421.

40. Tran, R., Xu, Z., Radhakrishnan, B., Winston, D., Sun, W., Persson, K.A., and Ong, S.P. (2016). Surface energies of elemental crystals. Sci. Data *3*, 160080.

41. Zhao, C.X., Bu, Y.F., Gao, W., and Jiang, Q. (2017). CO_2 reduction mechanism on the Pb(111) surface: effect of solvent and cations. J. Phys. Chem. C *121*, 19767–19773.

42. Hammer, B., Nielsen, O.H., and Nrskov, J.K. (1997). Structure sensitivity in adsorption: CO interaction with stepped and reconstructed Pt surfaces. Catal. Lett. *46*, 31–35.

43. Han, Y.J., Zhang, X., and Leach, G.W. (2014). Shape control of electrodeposited copper films and nanostructures through additive effects. Langmuir *30*, 3589–3598.

44. Liu, X., Xiao, J., Peng, H., Hong, X., Chan, K., and Nørskov, J.K. (2017). Understanding trends in electrochemical carbon dioxide reduction rates. Nat. Commun. *8*, 15438.

45. Tang, M.T., Ulissi, Z.W., and Chan, K. (2018). Theoretical investigations of transition metal surface energies under lattice strain and CO environment. J. Phys. Chem. C *122*, 14481–14487.